Tanzania Journal of Engineering and Technology 2025, **44**(3):69-85
OPEN ACCESS articles distributed under Creative Commons Attribution Licence [CC BY-ND]
Websites: https://commons.udsm.ac.tz/tjet/; https://ajol.org/tjet

ISSN 1821-536X (**print**); ISSN 2619-8789 (**electronic**)
https://doi.org/10.52339/tjet.v44i3.1042

Regular Research Manuscript

Maximum Likelihood Symbol Timing Algorithm Based on Cyclic Prefix for OFDM Systems

Kwame Ibwe

Department of Electronics and Telecommunications Engineering, University of Dar es Salaam, P.O BOX 33336 Dar es Salaam, Tanzania.
Corresponding Author: kwame.ibwe@udsm.ac.tz; ORCID: 0000-0003-4247-5154

ABSTRACT

In this paper, a blind symbol synchronization algorithm is presented for orthogonal frequency-division multiplexing (OFDM) systems, and a timing function based on the redundancy of the cyclic prefix (CP) is introduced. The existing algorithms rely on the prior knowledge of the channel energy distribution i.e. channel power profile. In practical environment the channel power profile is unknown to the receiver and its statistics are expected to be highly changing. Nevertheless, the use of pilot symbols in channel profile estimation reduces efficiency as data subcarriers are used to carry pilots instead of payload. In this paper a timing function that accounts for early and late timing introduced errors together with channel estimation errors is introduced. The effects of symbol timing errors are quantified and an optimal OFDM symbol timing solution is derived using modified maximum likelihood (ML) method. Compared with existing schemes in the literature, the proposed approach does not rely on explicit detection of individual channel paths or the delay spread boundary and therefore greatly reduces timing complexity. The main contribution lies in modifying the ML metric to jointly account for intercarrier interference (ICI), inter symbol interference (ISI), and channel estimation error, leading to improved robustness in dispersive channels without requiring prior channel knowledge. Simulation results show that the proposed algorithm is robust and outperforms the existing CP-based algorithms, particularly in double dispersive channels, achieving up to 5 dB NMSE improvement, lower BER at low SNR, and a 33% reduction in computational complexity.

ARTICLE INFO
Submitted: **Aug. 17, 2024**
Revised: **July 26, 2025**
Accepted: **Sep. 30, 2025**
Published: **Oct, 2025**

Keywords: *OFDM, Maximum Likelihood, Symbol Timing, Cyclic Prefix.*

INTRODUCTION

Multicarrier transmission has been successful method of increasing data transmission rate by using many parallel carriers each carrying relatively slow data rate. It is considered a promising technique for broadband wireless networks (Jin et al., 2023). The most used multicarrier technology is OFDM which has been widely used in wireless communications standards such as wireless LAN and digital video broadcasting - terrestrial (DVB-T) (D. Liu et al., 2022) . The third-generation partnership project (3GPP) launched 5G (fifth-generation mobile technology), a new standard for cellular networks in 2018 to replace the previous standards of 3G, 4G and 4G LTE (Jin et al., 2023). The objective was to define a new set of standards for devices and applications compatible with 5G networks(Ji et al., 2018). Like its predecessors, 5G uses radio waves to transmit data(Sarwar et al., 2023). However, because of improvements in latency, throughput and bandwidth, 5G networks can

reach much faster download and upload speeds, giving it a much wider range of applications (Chen et al., 2023). 5G release 17 achieves theoretical data rates for downlink (DL) and uplink (UL) of up to 100 Gbps and 1 Gbps respectively (Boodai et al., 2023). For 5G New Radio (NR), cyclic prefix OFDM (CP-OFDM) has been selected as the primary waveform for downlink transmission. This choice builds on the successful use of OFDM in 4G LTE, providing good spectral efficiency and resilience to selective fading(Yusof et al., 2023). While OFDM has been a foundational technology for 4G and is adapted for 5G, it does face challenges in time and frequency synchronization causing inter symbol (ISI) and intercarrier interferences (ICI)(Shammaa et al., 2024; Suyoto et al., 2021; C. Yang et al., 2024). Amid these advancements, accurate symbol timing synchronization remains a critical yet unresolved challenge in OFDM systems, especially under realistic channel conditions such as time and frequency dispersion(Tang, 2023).

In OFDM systems, synchronization issues are of great importance since synchronization errors might destroy the orthogonality among all subcarriers and, therefore, introduce inter-carrier interference (ICI) and inter-symbol interference(ISI) (Matin & Milstein, 2021). In this paper, symbol synchronization is the focus. The objective is to find the correct starting position [i.e., the fast Fourier transform (FFT) window] of the OFDM symbol for FFT demodulation. It is equivalent to estimate the timing offset between the transmitter and receiver. This is also referred to as timing synchronization. Note that the timing offset is an integer and can be anywhere within an OFDM symbol. Time offset estimation may be performed at the receiver using a predesigned preamble(Kang et al., 2008). Although accurate estimation can be achieved, the bandwidth efficiency is inevitably reduced. To eliminate this reduction, algorithms using the redundancy introduced by the cyclic prefix (CP) have been proposed(Ma et al., 2009; M. M. Wang et al., 2009; Yusof et al., 2023).The most famous one is the maximum likelihood (ML) symbol synchronization algorithm(Van De Beek et al., 1997). However, good performance is achieved only under flat-fading channels. When the system is operating under double dispersive fading channels, the ML algorithm exhibits significant fluctuation in the estimated timing offset. This is because the maximum of the timing function depends on channel conditions and does not necessarily point to the correct timing offset due to ISI, ICI and channel induced errors. Recently, a number of algorithms have been proposed in (Kalbat et al., 2022; Lin, 2018; T. Liu & Zhou, 2009; Yağlı & Aldırmaz Çolak, 2022; F. Yang & Zhang, 2024) to combat the effect of ISI and mitigate the fluctuation. Unfortunately, the double correlation method in (F. Yang & Zhang, 2024) works well only when the first path channels response is the strongest. The correlation derivative algorithm in (F. Yang & Zhang, 2024) makes use of the property that the correlator output is the sum of a set of triangular functions and is sensitive to the carrier frequency offset, as well as the filter length used. The asymptotic maximum likelihood (ML) algorithm in (Zhang & Liu, 2023) uses the correlation length equal to the sum of the channel and CP lengths. It is rather impractical since exact knowledge of the channel power profile and channel length is required. The algorithms in (Kalbat et al., 2022; Nasir et al., 2010; Peng et al., 2023; M. M. Wang et al., 2009) rely on the prior knowledge of the channel energy distribution i.e. channel power profile. These methods, while effective under constrained assumptions, often struggle with timing ambiguity or require impractical knowledge of channel statistics, limiting their deployment in fast-changing or unknown environments.

In practical environment the channel power profile is unknown to the receiver and its statistics are expected to be highly changing(J. Yang et al., 2020). Indeed, the flexibility in FFT window placement in a single tap channel is not present with double dispersive channels(Ling & Proakis, 2017). The long delay spread can make it difficult, if not impossible, to fit all delayed OFDM symbol replicas from different channel taps into one FFT window without causing signal distortion, even with a known delay spread boundary(Peng et al., 2023). Recent works, such as convolutional neural network (CNN) and deep learning-based synchronization techniques, highlight the trend toward data-driven methods, but often suffer from generalization and training data limitations(Kojima et al., 2023). In this paper, the effects of timing offset are quantified and an optimal OFDM symbol timing solution using modified ML algorithm is derived. This

is achieved by maximizing the ratio between average subcarrier signal power and average subcarrier interference. This method eliminates the need to detect the boundary of the channel delay spread. It also provides a close to optimal FFT window position even in the presence of channel delay spread longer than the CP.

METHODS AND MATERIALS

OFDM Signal Model

Consider a simplified block diagram of a general multicarrier system in Figure 1. The list of symbols and notations used to derive the robust timing estimator is detailed in Table 1.

Table 1: List of Symbols and Notations

Symbol	Description
N	Number of subcarriers (FFT size)
G	Length of the cyclic prefix (CP)
J	Total OFDM symbol length after CP insertion, $J = N + G$
t_d	Time offset (in number of samples)
$h(n)$	Discrete time channel impulse response
$r(n)$	Received time-domain signal
$\mathbf{H}$	$N \times N$ frequency-domain channel matrix
$\mathbf{E}$	Equalizer $J \times N$ matrix at the receiver
$\mathbf{F}$	$N \times N$ IFFT matrix
$\bar{\mathbf{F}}_1$	$G \times N$ matrix formed by last G rows of $\mathbf{F}$
$\bar{\mathbf{F}}$	$N \times N$ IFFT matrix
$\boldsymbol{a(n)}$	Transmitted frequency-domain symbol (input to IFFT)
$\boldsymbol{s(n)}$	Time-domain transmit signal (output of IFFT with CP insertion)
ϵ	Normalized carrier frequency offset (CFO)
$\boldsymbol{\gamma(t_d)}$	Timing detection metric used in ML estimation
$SIR\ (t_d)$	Signal-to-interference ration as a function of timing offset
$NMSE$	Normalized mean square error

The information symbols $a(n)$ are first serial to parallel (S/P) converted to $N \times 1$ vectors $a(i) \triangleq [a(iN)\ a(iN+1)\ \ldots\ a(iN+N-1)]^T$. N is usually the number of subcarriers used or the FFT matrix size and $i \in 0,1,2,3,\ldots N-1$. These vectors are modulated by $J \times N$ matrix $\mathbf{F}$. $\mathbf{F} = [\bar{\mathbf{F}}_1{}^{\mathrm{T}},\ \bar{\mathbf{F}}^{\mathrm{T}}]^{\mathrm{T}}$, where $\bar{\mathbf{F}}$ is the $N \times N$ Inverse Fast Fourier Transform (IFFT) matrix with entries $[\bar{\mathbf{F}}]_{k,l} \triangleq \mathrm{N}^{-1/2}\exp(j2\pi(k-1)(l-1))$ for k row and l column. $\bar{\mathbf{F}}_1$ is the J-$N \times N$ matrix formed from the last J-N rows of $\bar{\mathbf{F}}$. J is chosen to avoid multipath – induced inter symbol interference (ISI) i.e. $J \geq N + L$ and L is the channel length.

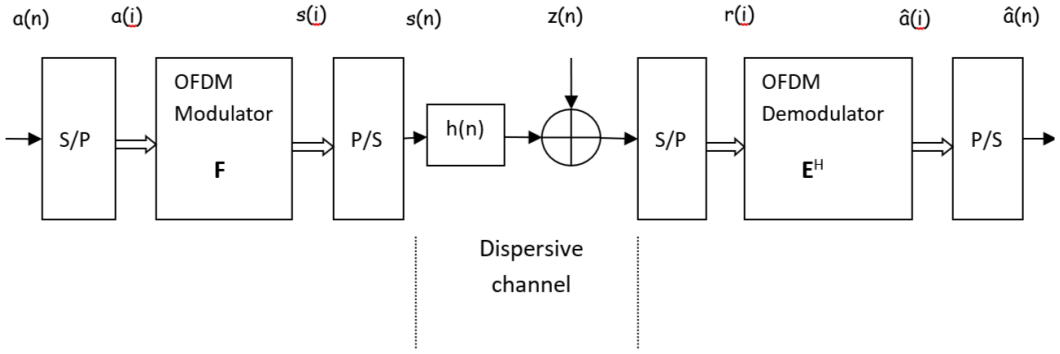

Figure 1: Baseband discrete time model of a general multicarrier system.

Technically, the block with function $\mathbf{F}$ performs the IFFT and cyclic prefix (CP) insertion automatically i.e. $s(i) = \mathbf{F}a(i)$. These data symbols (blocks), $s(i)$, are then parallel to serial (P/S) converted and sent through a doubly dispersive channel with impulse response $h(n)$. At the receiver the received samples $r(n)$ are S/P converted to $J \times 1$ vectors $r(i) \triangleq [r(iJ)\ r(iJ+1)\ \ldots\ r(iJ+J-1)]^T$ and then

equalized by the *J x N* matrix **E** to form $\hat{a}(i) = \mathbf{E}^H r(i)$. The equalizer matrix **E** is assumed to implement linear frequency-domain equalization based on estimated channel matrix **H**, with perfect synchronization assumed except for the timing offset under analysis.

At time index *n* the received signal is given as

$$r_n = \boldsymbol{h} \otimes s_{n-t_d} e^{\frac{j2\pi\varepsilon n}{N}} + z_n \qquad (1)$$

where **h** is the channel impulse response, s_n the transmit symbols (FFT of the data symbols), t_d denotes the integer valued channel delay, ε is the normalized carrier frequency offset (CFO) and z_n are complex valued, zero mean with unity variance ($\sigma_z{}^2 = 1$) noise samples.

However, due to CP inserted in front of the transmit symbols as shown in Figure 2, the linear convolution in equation 1 becomes circular convolution (Yli-Kaakinen et al., 2021). Hence, equation 1 can be written as;

$$r_n = \mathbf{H} s_{n-t_d} e^{\frac{j2\pi\varepsilon n}{N}} + z_n \qquad (2)$$

where **H** is N x N channel matrix. Equation 2 for received signal assumes no timing offset in placing the FFT window during demodulation at the receiver. If there is timing offset $t_d > G$, where G is the number of samples in the CP region and ignoring the noise samples, equation 2 can be written as;

$$r_n = \mathbf{H} \begin{bmatrix} s_{n-1}(N-(t_d-G)) \\ \vdots \\ s_{n-1}(N-1) \\ s_n(N-G) \\ \vdots \\ s_n(N-1) \\ s_n(0) \\ \vdots \\ s_n(N-1-t_d) \end{bmatrix} . e^{\frac{j2\pi\varepsilon n}{N}} + z_n \qquad (3)$$

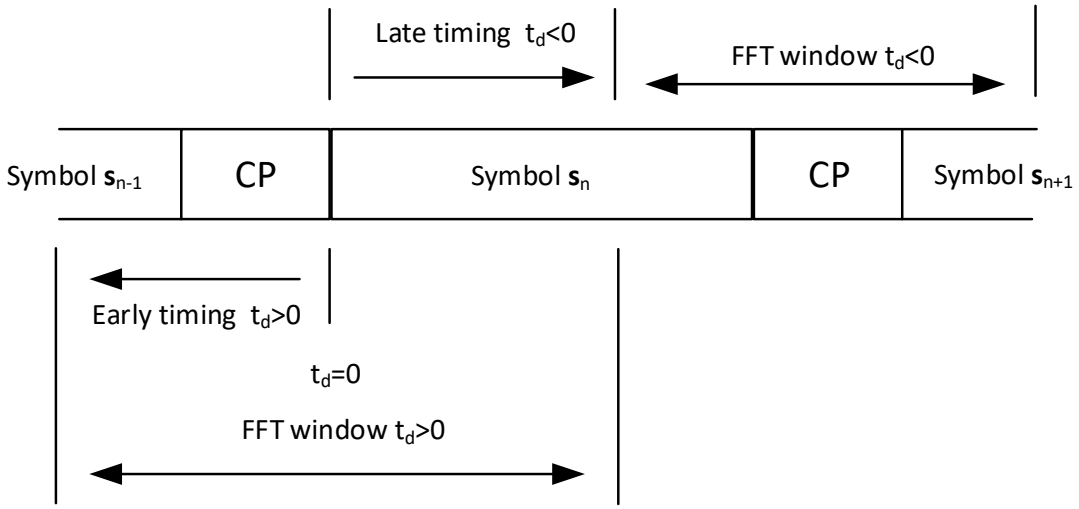

Figure 2: Timing offset definition for early and late timing.

Equation 3 can be broken down into three part as

$$r_n = \left[\mathbf{H} \begin{bmatrix} s_n(N-t_d) \\ \vdots \\ s_n(N-G+1) \\ s_n(N-G) \\ \vdots \\ s_n(N-1) \\ s_n(0) \\ \vdots \\ s_n(N-1-t_d) \end{bmatrix} - \mathbf{H} \begin{bmatrix} s_n(N-t_d) \\ \vdots \\ s_n(N-G+1) \\ 0 \\ \vdots \\ 0 \\ 0 \\ \vdots \\ 0 \end{bmatrix} \right. \\ \left. + \mathbf{H} \begin{bmatrix} s_{n-1}(N-(t_d-G)) \\ \vdots \\ s_{n-1}(N-1) \\ 0 \\ \vdots \\ 0 \\ 0 \\ \vdots \\ 0 \end{bmatrix} \right] . e^{\frac{j2\pi\varepsilon n}{N}} + z_n \quad (4)$$

It is observed that the first term in equation 4 is the cyclic shift of s_n and the second and third parts are interferences. Since the transmit symbols s_n are in time domain given as $s_n = \mathbf{F}^H a_n$, where **F** is the N x N FFT matrix, equation 4 can thus be written as

$$r_n = [\mathbf{F}^H \mathbf{H} a_n - \Delta \mathbf{F}^H \mathbf{H} a_n + \Delta \mathbf{F}^H \mathbf{H} a_{n-1}] . e^{\frac{j2\pi\varepsilon n}{N}} + z_n \quad (5)$$

where Δ is an identity matrix of size N with null diagonal elements from $N-(t_d-G)$ to N. It can be clearly seen that $r_n = \mathbf{F}^H \mathbf{H} a_n . e^{\frac{j2\pi\varepsilon n}{N}} + z_n$ if $0 \le t_d \le G$. That is there is no timing introduced error, except a phase ambiguity in the effective channel which can be removed by channel estimation, as long as the start of the FFT collection window is inside the cyclic prefix $0 < t_d \le G$ or at the start of the OFDM symbol $(t_d = 0)$. Observing the interferences in equation 5, the second and third terms are the intra symbol interference and inter symbol interference respectively. Intra symbol interference happens within the symbol itself among the different subcarriers and eventually led to inter carrier interference (ICI). The inter symbol interference is due to leakage of the previous symbol in the current symbol. To study the effect of intra symbol interference, the third term is omitted in equation 5. Then, the FFT of the remaining equation is given as

$$FFT\{r_n\} = R_k = FFT\{\mathbf{F}^H \mathbf{H} a_n - \Delta \mathbf{F}^H \mathbf{H} a_n\} \quad (6)$$

Therefore, equation 6 can be expressed as

$$R_k = \mathbf{H} a_n - \mathbf{F} \Delta \mathbf{F}^H \mathbf{H} a_n = (\mathrm{I} - \mathbf{F} \Delta \mathbf{F}^H) \mathbf{H} a_n \quad (7)$$

Equation 7 can be reformulated as

$$R_k = \Sigma \begin{bmatrix} 0 \\ \vdots \\ 0 \\ a_n(k) \\ 0 \\ \vdots \\ 0 \end{bmatrix} + \Sigma \begin{bmatrix} a_n(0) \\ \vdots \\ a_n(k-1) \\ 0 \\ a_n(k+1) \\ \vdots \\ a_n(N-1) \end{bmatrix} \quad (8)$$

where $\Sigma = (\mathrm{I} - \mathbf{F} \Delta \mathbf{F}^H) \mathbf{H}$. For the k[th] subcarrier of R_k at time n equation 8 can be written as

$$R_k[k] = \Sigma[k,k] a_n[k] + \sum_{\mathrm{i} \neq \mathrm{k}} \Sigma[k,i] a_n[i] \quad (9)$$

The first term is the scaling effect on subcarrier k and the second term is the inter-subcarrier interference or ICI on the subcarrier k. To estimate the total ICI power, the N x N covariance matrix of equation 7 has to be estimated first as;

$$\begin{aligned} & C_{ICI}(x) \\ & = \mathbb{E}\{\mathbf{H}a_n \\ & - \mathbf{F}\Delta\mathbf{F}^H\mathbf{H}a_n(\mathbf{H}a_n \\ & - \mathbf{F}\Delta\mathbf{F}^H\mathbf{H}a_n)^H\} \end{aligned} \quad (10)$$

Equation 10 can be reduced further by taking the like terms aside as

$$C_{ICI}(x) = \mathbb{E}\{|h|^2\}\left(\acute{\Sigma} - \acute{\Sigma}^2\right) \quad (11)$$

where $\acute{\Sigma} = (\mathrm{I} - \mathbf{F}\Delta\mathbf{F}^H) \approx \frac{t_d - G}{N}$. The ICI power on the k^{th} subcarrier is then given as

$$\begin{aligned} \sigma^2{}_{ICI}(t_d) = \mathbb{E}\{|h|^2\}\Bigg(&\frac{t_d - G}{N} \\ &- \left(\frac{t_d - G}{N}\right)^2\Bigg) \end{aligned} \quad (12)$$

Equation 12 for ICI power holds only for early timing i.e. $t_d > 0$, to account for both late and exact timing, equation 12 can be written as

$$\sigma^2{}_{ICI}(t_d) = \mathbb{E}\{|h|^2\}\alpha_{ICI}(t_d) \quad (13)$$

where the ICI density function is given as

$$\alpha_{ICI}(t_d) = \begin{cases} \frac{|t_d|}{N} - \frac{|t_d|^2}{N^2} & -N \le t_d < 0 \\ 0 & 0 \le t_d \le G \\ \frac{t_d - G}{N} - \left(\frac{t_d - G}{N}\right)^2 & G < t_d < G - \\ 0 & Otherwise \end{cases} \quad (14)$$

Inter symbol interference (ISI) power in equation 5 is calculated in similar manner by estimating the covariance matrix of the FFT of ISI term as

$$\begin{aligned} & C_{ISI}(t_d) = \\ & \mathbb{E}\{\mathbf{F}\Delta\mathbf{F}^H\mathbf{H}a_{n-1}(\mathbf{F}\Delta\mathbf{F}^H\mathbf{H}a_{n-1})^H\} = \\ & \mathbb{E}\{|h|^2\}\mathbf{F}|\Delta|^{\mathbf{2}}\mathbf{F}^H \end{aligned} \quad (15)$$

The ISI power on the k[th] subcarrier can then be represented as

$$\sigma^2{}_{ISI}(t_d) = \mathbb{E}\{|h|^2\}\left(\frac{t_d - G}{N}\right) \quad (16)$$

But, equation 16 holds for early timing only, to generalize for both early, exact and late timing equation 16 can be written as

$$\sigma^2{}_{ISI}(t_d) = \mathbb{E}\{|h|^2\}\alpha_{ISI}(t_d) \quad (17)$$

where the ISI density function is given as

$$\alpha_{ISI}(t_d) = \begin{cases} \frac{|t_d|}{N} & -N \le t_d < 0 \\ 0 & 0 \le t_d \le G \\ \frac{t_d - G}{N} & G < t_d < G + N \\ 1 & Otherwise \end{cases} \quad (18)$$

To completely characterize the impact of timing error on the performance of OFDM symbol demodulation, the effect of channel estimation on the timing decision must be included. The channel estimation error should also be examined in the three cases as the ISI and ICI. Considering the first case of the late timing where $t_d < 0$, i.e. the channel taps arrive prior to the FFT window as a result of late timing, the mean interference variance due to channel estimation error is;

$$\sigma^2{}_{CE}(t_d) = 2E\{|h|^2\}\left(1 + \frac{t_d}{N}\right) \quad (19)$$

For the case of early timing, $t_d > 0$, the mean channel interference error variance will be;

$$\begin{aligned} \sigma^2{}_{CE}(t_d) = 2E\{|h|^2\}\Bigg(&1 \\ &- \frac{t_d - G}{N}\Bigg) \end{aligned} \quad (20)$$

Based on the analysis above the total timing error variance is the sum of the three error terms for ISI, ICI and channel estimation error. Hence for timing offset of t_d the total error variance will be;

$$\begin{aligned} \sigma^2{}_{total}(t_d) = &\sigma^2{}_{ISI}(t_d) \\ &+ \sigma^2{}_{ICI}(t_d) \\ &+ \sigma^2{}_{CE}(t_d) \end{aligned} \quad (21)$$

The received signal power is also estimated from equation 9. Taking the expectation of the first term in equation 9 yields;

$$E\{R_n\} = E\{\Sigma[k,k]a_n[k](\Sigma[k,k]a_n[k])^H\} \quad (22)$$

The received signal power with timing offset of t_d is then given as;

$$\sigma^2{}_{R_n}(x) = E\{|h|^2\}\left(\frac{x-G}{N}\right)^2 R_{aa} \quad (23)$$

where R_{aa} is the covariance matrix of information symbols. From (21) the resultant power attenuation factor for the k^{th} subcarrier is;

$$\alpha^2(t_d) = E\{|h|^2\}\left(\frac{t_d-G}{N}\right)^2 \quad (24)$$

Equation (24) quantifies the impact of timing offset on received power at the subcarrier level. Results in (24) enable the computation of signal-to-interference ratio (SIR) needed for evaluating synchronization accuracy. Therefore, the SIR associated with the collected OFDM symbol at time offset t_d is then given as;

$$SIR(t_d) = \frac{\sigma^2{}_{R_k}(t_d)}{\sigma^2{}_{total}(t_d)} = \frac{\sum_i E\{|h|^2\}\left(\frac{i-G}{N}\right)^2 R_{aa}}{\sum_i E\{|h|^2\}\left(2\left(1+\frac{2t_d}{N}\right)-\frac{{t_d}^2}{N^2}\right)} \quad (25)$$

for $i \in \{-t_d, -t_d+1, \dots, 0, \dots, N+G+t_d\}$.

Robust Timing Estimator

Considering the maximum likelihood parameter estimation (Fazel & Kaiser, 2008), the joint maximum likelihood estimate of $f_{CFO} = \epsilon * \frac{1}{NT}$ and t_d, the frequency and timing error respectively, is given as

$$LLF(f_{CFO}, t_d) = \log \mathrm{p}(r|f_{CFO}, t_d) \quad (26)$$

where $\mathrm{p}(r|f_{CFO}, t_d)$ denotes the probability density function of observing the received signal r given as frequency error f_{CFO} and timing error t_d. It is shown in (Fazel & Kaiser, 2008) that for $N+X$ samples;

$$LLF(f_{CFO}, t_d) = |\gamma(t_d)|\cos\left(2\pi f_{CFO} + \angle\gamma(t_d)\right) - \rho\Phi(t_d) \quad (27)$$

where

$$\gamma(k) = \sum_{k=1}^{X-1} r_n(k){r_n}^*(k+N) \quad (28)$$

and

$$\Phi(k) = \sum_{k=1}^{X-1} |r_n(k)|^2 + |r_n(k+N)|^2 \quad (29)$$

X is any integer and ρ is a constant depending on the SNR which represents the magnitude of the correlation between the sequences *r(k)* and *r(k + N)*. Note that the first term in equation 26 is the weighted-magnitude of *γ (t$_d$)*, which is the sum of *X* consecutive correlations. These sequences *r(k)* could be known in the receiver by exploiting the presence of the guard time $(k = G)$. The maximization of the log likelihood function (LLF) in equation 26 can be done in two steps: first, maximization can be performed to find the frequency error estimate $\hat{f}_{CFO}$, and then, exploit it for final maximization to find the timing error estimate t_d. The maximization of $\hat{f}_{CFO}$ is given by the partial derivative of equation 26 as $\partial LLF(\hat{f}_{CFO}, t_d)/\partial\hat{f}_{CFO} = 0$, which results in:

$$\hat{f}_{CFO} = -\frac{1}{2\pi}\angle\gamma(t_d) + \varpi = -\frac{1}{2\pi}\frac{\sum_{k=x}^{x+X-1} Im[r_n(k){r_n}^*(k+N)]}{\sum_{k=x}^{x+X-1} Re[r_n(k){r_n}^*(k+N)]} + \varpi \quad (30)$$

where ϖ is an integer value. By inserting $\hat{f}_{CFO}$ in equation 26, it yields

$$LLF(\hat{f}_{CFO}, t_d) = |\gamma(t_d)| - \rho\Phi(t_d) \quad (31)$$

and maximizing equation 31 gives a joint estimate of $\hat{f}_{CFO}$ and t_d ;

$$\hat{f}_{CFO} = -\frac{1}{2\pi}\angle\gamma(t_d) \quad (32)$$

$$t_d = arg\left(\max_{t_d}\{|\gamma(t_d)| - \rho\Phi(t_d)\}\right) \quad (33)$$

The main drawbacks of the maximum likelihood frequency detection above are the small range of acquisition which is only half of the sub-carrier spacing $\frac{1}{2NT}$ and fixed width of timing offset detection i.e. $t_d \in [0, 1, 2, \dots, N+G]$. When $\hat{f}_{CFO} \to \frac{1}{2NT}$, the estimate $\hat{f}_{CFO}$ may, due to noise and the discontinuity of arctangent, jump to -0.5. When this happens, the estimate is no longer unbiased and in practice it becomes useless. And when $t_d < 0$ the algorithm cannot detect accurately the early timing as analyzed in (M. M. Wang et al., 2009). Thus, for frequency errors exceeding one half of the sub-carrier spacing, an initial acquisition strategy, coarse frequency acquisition, should be applied. To enlarge the acquisition range of a maximum likelihood estimator, a modified version of this estimator is proposed below. The new timing function is now proposed as

$$\Gamma(k,m) \triangleq \left|\sum_{k=t_d}^{N+G-1}\sum_{n=m}^{G-1} E\{r(n+k)r^*(n+k+N)\}\right| - \frac{SIR(t_d)^2}{2}\sum_{k=t_d}^{N+G-1}\sum_{n=m}^{G-1}[E\{|r(n+k)|^2\} + E\{|r(n+k+N)|^2\}] \quad (34)$$

where $t_d \in \left\{-\frac{N}{2}, -\frac{N}{2}+1, \dots, 0, \dots, N+G-1\right\}$; $m \in \{0,1,\dots,G-1\}$

with the assumption that early timing will be not more than half the previous symbols samples. Substituting equation 25 into equation 34 yields the new timing function as

$$\Gamma(k,m) \triangleq \left|\sum_{k=t_d}^{N+G-1}\sum_{n=m}^{G-1} E\{r(n+k)r^*(n+k+N)\}\right| - \frac{\left(\frac{\sum_i E\{|h|^2\}\left(\frac{i-G}{N}\right)^2 R_{aa}}{\sum_i E\{|h|^2\}\left(2\left(1+\frac{2t_d}{N}\right)-\frac{{t_d}^2}{N^2}\right)}\right)^2}{2}\sum_{k=t_d}^{N+G-1}\sum_{n=m}^{G-1}[E\{|r(n+k)|^2\} + E\{|r(n+k+N)|^2\}] \quad (35)$$

where $t_d \in \left\{-\frac{N}{2}, -\frac{N}{2}+1, , 0, 1, , N+G-1\right\}$; $m \in \{0,1,\dots,G-1\}$; $i \in \{-t_d, -t_d+1, \dots, 0, \dots, N+G+t_d\}$

The proposed estimator operates by scanning over a predefined timing window, typically bounded by the cyclic prefix length and computing the timing metric in equation (35) for each candidate offset. Initialization involves selecting a coarse estimate of the search range based on CP duration and expected delay spread. For large timing offsets, the method's reliance on interference-based SIR rather than explicit channel detection enables reliable alignment without prior synchronization. Under low SNR, robustness is maintained by averaging over subcarriers, which smooths noise impact in the timing metric. The estimator can be implemented using standard FFT/IFFT operations and covariance estimation over a small number of OFDM blocks.

EXPERIMENTAL RESULTS

Simulation Parameters

In this section, the parameters for simulation analysis of the proposed symbol time estimation algorithm based on the modified maximum likelihood (ML) algorithm are presented. The proposed method is compared with the symbol

timing scheme presented in (Kojima et al., 2023) and (Y. C. Wang & Phoong, 2017). The method presented in (Kojima et al., 2023) uses supervised convolutional neural network (CNN) based symbol timing synchronization method. In (Y. C. Wang & Phoong, 2017) the authors used constant modulus (CM) constellation method to track the symbol time offset. The two methods are selected as baselines because they represent two dominant and contrasting approaches to blind synchronization in OFDM: a modern data-driven method (CNN-based) and a classical signal-structure-based method (CM-based). Additionally, both are among the few existing schemes evaluated under doubly dispersive channels, making them suitable for benchmarking the proposed method in realistic and challenging environments. Table 2 shows the system and timing experimental conditions based on the 3GPP standard in the numerical experiments.

Table 2: Simulation and Experimental Conditions

Parameter	Value
Subcarrier spacing (ε)	$\frac{1}{4}$
OFDM symbol duration	$\frac{1}{30}$ ms
FFT-points N	512
Carrier frequency	2.15GHz
Sampling interval T_s	72 μ s
Modulation	QPSK
CP length (G)	64
Subcarrier mapping ($\boldsymbol{K \leq N}$)	$-\frac{K}{2}, -\frac{K}{2} + 1, \ldots\ldots, \frac{K}{2} - 1$
Transmission bandwidth	5 MHz 10 MHz

As a metric of the symbol time estimation accuracy, the normalized mean square error (NMSE) is defined as

$$NMSE = E\left\{\frac{\|\hat{t}_d - t_d\|^2}{\|t_d\|^2}\right\} \qquad (36)$$

where t_d is the true value and $\hat{t}_d$ is the estimated symbol timing value. The signal to noise power ratio (SNR) of the channel is defined as

$$SNR_{dB} = 10log10\left(\frac{\mathrm{E}\{\|r_k\|^2\}}{\mathrm{E}\{\|z_k\|^2\}}\right) \qquad (37)$$

In this work the bandwidth of transmission is assumed to be equal to the data rate. Therefore, the SNR defined in (24) can also be represented as

$$SNR_{dB} = 10log10\left(\frac{E_b}{N_0}\right) \qquad (38)$$

where E_b and N_0 are energy per bit and noise power spectral density.

For simulation, 10000 random symbols are generated and the system utilizes the IDFT transform with QPSK constellations. The channel is simulated as a L+1=11 tap FIR channel and is assumed that the channel taps are independent and identically distributed (i.i.d.) and correlate in time. The timing offset was set to two hundred samples periods (t_d=100) and the SNR was set to be 10dB. The doubly dispersive channel model used is the one presented in (Ling & Proakis, 2017), with channel order of 10 (L=11). A total of 10,000 Monte Carlo trials are performed for each simulation point to ensure statistical reliability. Extreme timing offsets are handled by defining a search window that spans the entire CP duration and part of the symbol duration, ensuring coverage of early, exact, and late timing cases.

RESULTS AND DISCUSSION

The timing detection metric versus SNR is depicted in Figure 3 when 2 x 2 MIMO configuration is used in doubly dispersive channel. The timing offset detection metric reported in equation 35 takes the shape of a triangular pulse at the timing offset, therefore indicating the beginning of the symbol. The timing detection is conducted in doubly dispersive channel at SNR of 5dB. The comparison is done with existing works in (Kojima et al., 2023) and (Y. C. Wang & Phoong, 2017). Results show that proposed method is sharper at the timing

offset of 200 samples compared to the existing works. The method presented in (Kojima et al., 2023) has inaccuracy of 50 samples while the work in (Y. C. Wang & Phoong, 2017) exhibit inaccuracy of 200 samples. Detection accuracy comparison is repeated in Figure 4 and Figure 5 at SNR levels of 10dB and 20dB respectively. In both cases the proposed methods outperform the existing works with a sharper detection lobe at the 200 samples mark. In the synchronization process, detection of the beginning of the symbol is a significant step in establishing the symbol time offset. The proposed time detection metric in equation 35 converges well at the time offset mark demonstrating its robustness over the existing method.

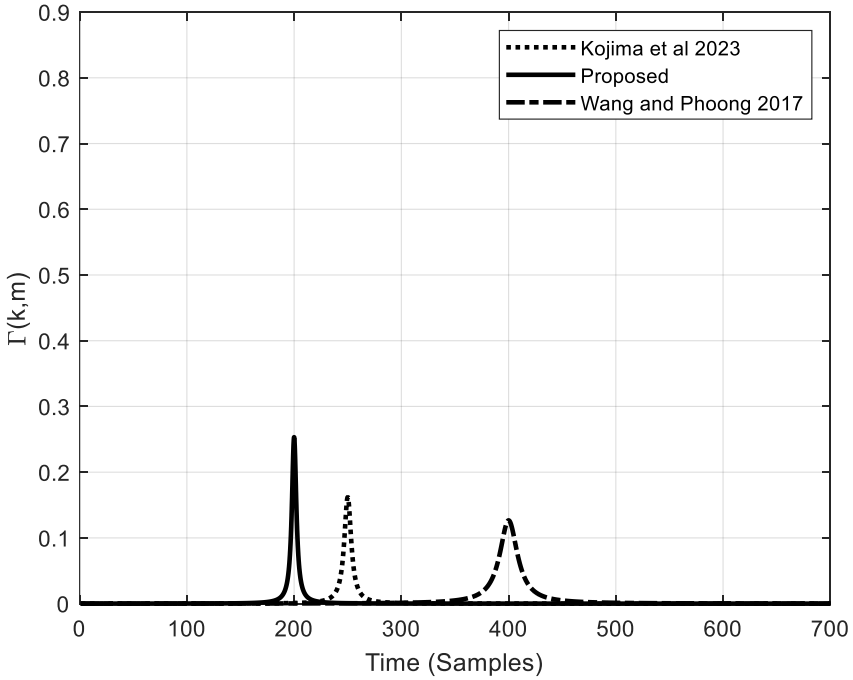

Figure 3: Time detection metric in doubly dispersive channel at SNR =5dB.

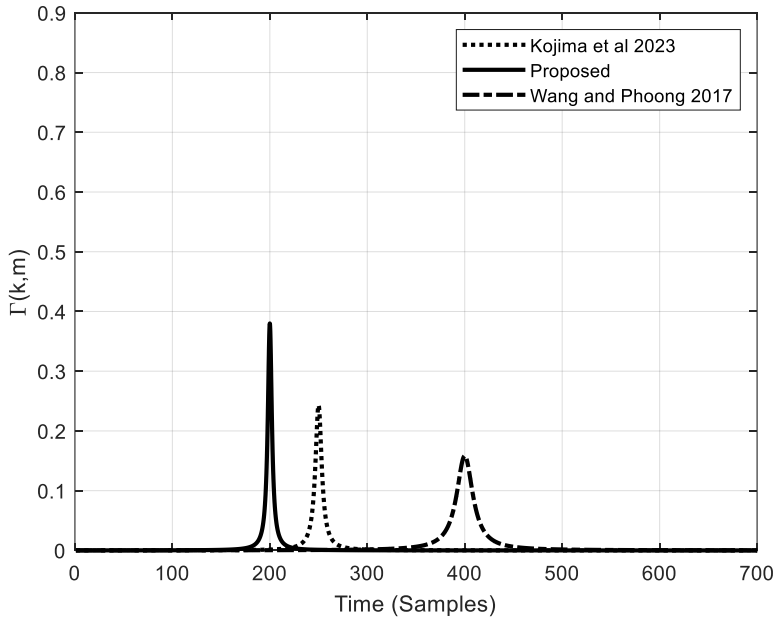

Figure 4: Time detection metric in doubly dispersive channel at SNR =10dB.

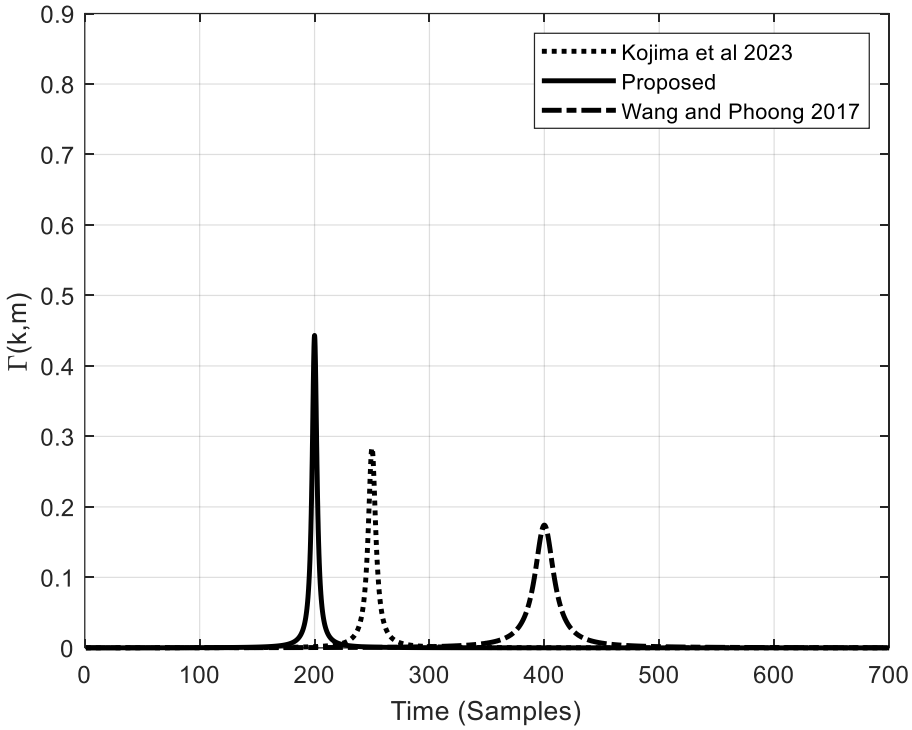

Figure 5: Time detection metric in doubly dispersive channel at SNR =20dB

In order to verify the usefulness of the proposed synchronization method, the simulations are conducted for OFDM system using the parameters shown in Table 1. The performance of the existing and proposed symbol timing estimation methods are compared as shown in Figure 6 and Figure 7. Figure 6 shows the normalized mean square error (NMSE) performance of the timing detection method when 2 x 2 multi input multi output (MIMO) antenna configuration is used. In this setup, the performance comparison between the existing and proposed method is presented. It is observed that under doubly dispersive channel conditions, the MSE of the proposed estimation scheme is lower than that of the existing estimation schemes. Since the side lobe of the timing detection metric is reduced as previously observed in Figure 3, Figure 4 and Figure 5, the proposed scheme achieves much better estimation over fading channels. In Figure 7, the NMSE performance of the symbol timing detection schemes for 2 x 4 MIMO configuration is depicted under the same conditions as in Figure 6. The relative performance of the existing and proposed estimation methods is observed to be improved by 5dB to that presented in Figure 6. As expected, the diversity gain is improved with the increase in the number of receive antenna and consequently improving the estimation capability of the synchronization schemes. The proposed method achieves a detection accuracy of ±0 samples at the true timing offset under 5 dB SNR, compared to ±50 and ±200 samples for the CNN and CM based methods, respectively. This translates to a 25% to 100% reduction in timing offset estimation error under low SNR. Similarly, Figure 6 and Figure 7, the observed NMSE gain of 5 dB corresponds to accurate symbol alignment, which directly benefits demodulation and decoding performance. These improvements are valuable for uplink synchronization in 5G massive MIMO systems, where poor timing estimation propagates errors in channel estimation and reduce spectral efficiency.

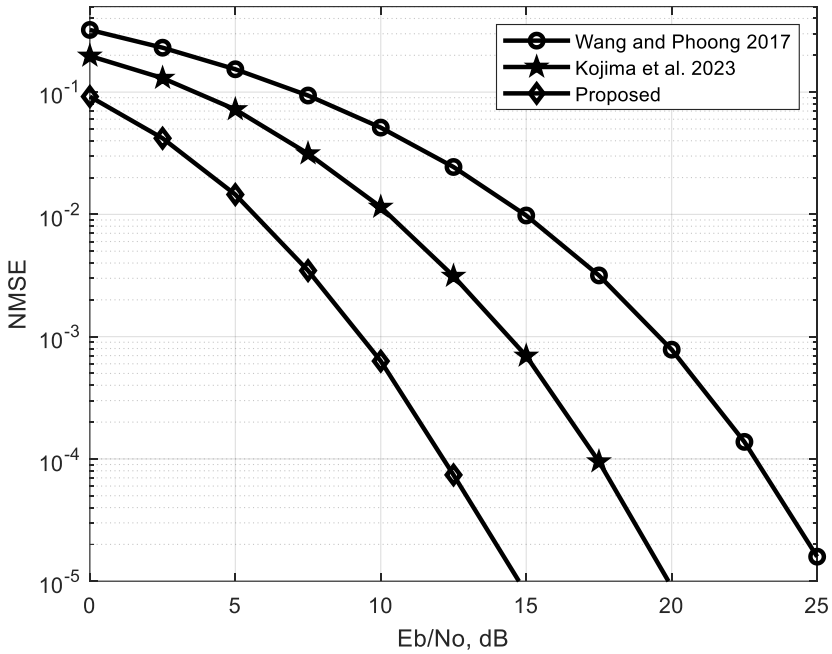

Figure 6: MSE vs SNR for proposed and existing timing methods with 2 x 2 MIMO.

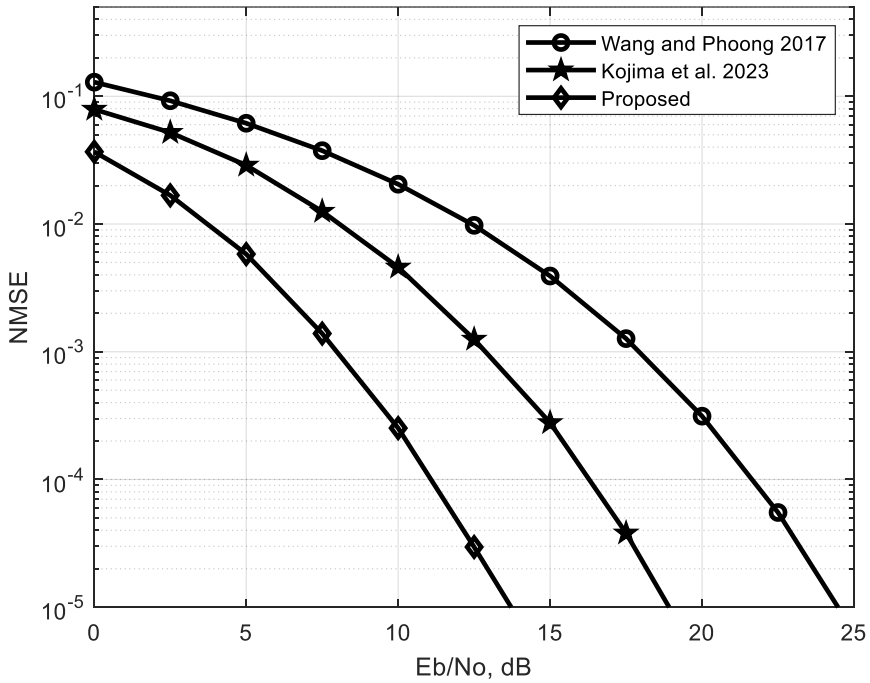

Figure 7: MSE vs SNR for proposed and existing timing methods with 2 x 4 MIMO.

The observed 5 dB NMSE improvement when moving from 2×2 to 2×4 MIMO is attributed to spatial diversity gain. With more receive antennas, the system benefits from improved averaging over independent channel realizations, which reduces sensitivity to noise and channel estimation errors. The increased spatial degrees of freedom enhance the receiver's ability to suppress inter-symbol and inter-carrier interference, leading to more accurate symbol timing detection.

For fair comparison between proposed and existing OFDM symbol timing estimation

schemes, the computational complexity is presented in Table 2. The complexity in this study is defined as of the number of multiplications, additions, matrix inversions and computational resources needed to complete each estimation. N_s is the number of symbols, N_{CP} is the CP length, N is the number of subcarriers and R^{-1} is the inverse of received signal matrix.

Table 2: Complexity of symbol timing schemes

Scheme	Complexity	Processing Time [ms]	BER (Eb/No=25dB)
Wang and Phoong et al. 2017	$O(N_{CP}N_S(N+N_{CP}))$	13.50	0.00342
Kojima et al., 2023	$O(N_{CP}N_S(N+N_{CP})*R^{-1})$	12.10	0.000456
Proposed	$O(N_{CP}N_SN)$	9.02	0.000302

The processing time is the average estimation time of 10,000 trials in the simulation environment presented in Table 1. As observed in Table 2, the proposed method converges faster than existing methods with low computational complexity. For existing schemes, the computational resources required grow proportionally to the product of number of subcarriers, number of cyclic prefix, number of symbols and inverse of the receive signal matrix.

The BER performance of the OFDM system using the proposed scheme is compared with existing ones in Figure 8 and Figure 9 under the 2 x 2 and 2 x 4 MIMO configurations respectively. From Figure 8 it is observed that as the signal power increases, the bit error rate decreases indicating higher probability of estimation accuracy. The proposed scheme demonstrates energy efficiency by achieving lower BER performance at low SNR values. In Figure 9, the increased diversity gain is observed to be exploited well by the existing scheme by achieving a 7dB improvement in BER performance under the same channel conditions.

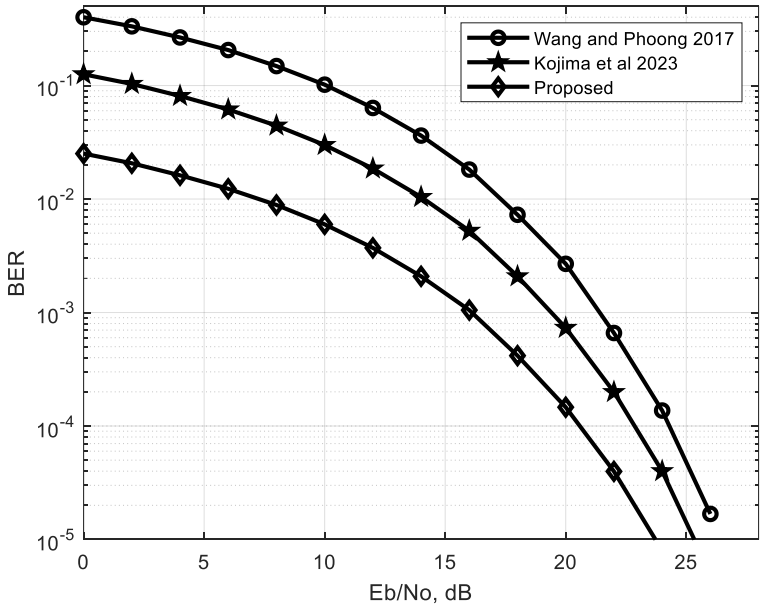

Figure 8: BER vs SNR for proposed and existing timing methods with 2 x 2 MIMO.

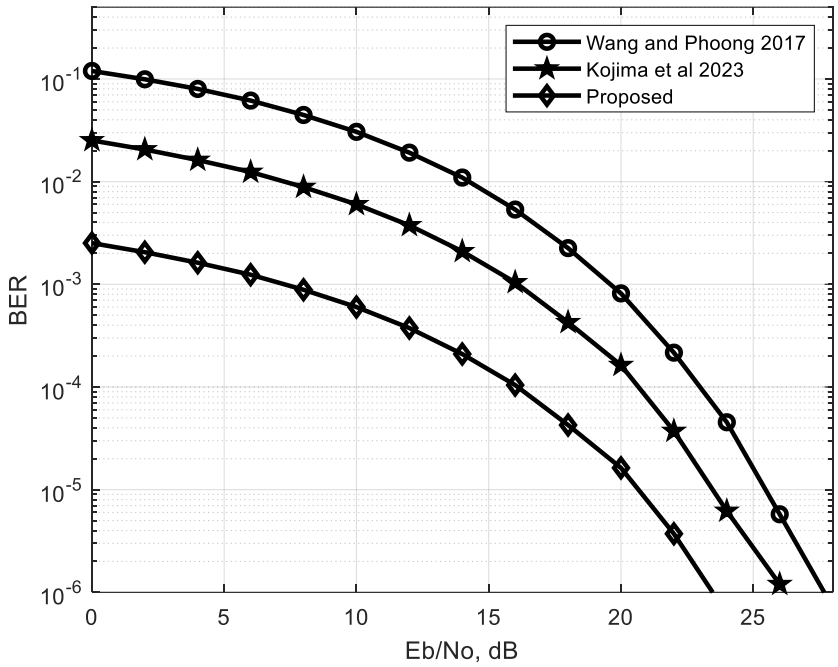

Figure 9: BER vs SNR for proposed and existing timing methods with 2 x 4 MIMO.

The presented simulation results for the proposed method have practical implications for real-world MIMO OFDM systems. The hybrid method's ability to maintain low BER in highly changing channels makes it suitable for various applications, including wireless broadband and 5G networks. In the case where such strict timing estimation is required, conventional ML almost result in erroneous judgments, leading to low error rate performance. CNN is a method that uses an autocorrelation function for estimation, and CM further considers the additive noise effect on conventional ML. These methods are greatly affected by ISI and ICI. As a result, synchronization errors unacceptably occur, and it causes error floors regardless of the Eb/No value. The proposed method show superior error rates, especially at a low Eb/No, because the peak values required for timing estimation can be accurately obtained thanks to the reduced influence of the noise term. These findings guide the design of robust communication systems and highlight the modified ML method's practical advantages over the conventional ML, CNN and CM methods.

CONCLUSIONS

In this paper, results presented demonstrate the effectiveness of the proposed timing detection metric for MIMO configurations in doubly dispersive channels. The method consistently outperforms existing techniques, achieving up to 5 dB NMSE improvement, ±0 sample timing accuracy at 5 dB SNR, and a 33% reduction in processing time compared to CNN- and CM-based baselines. The sharper detection peak at the correct timing offset improves demodulation reliability across all evaluated SNR levels. Additionally, the proposed method exhibits a significant reduction in computational complexity and processing time, making it more efficient for real-world applications. The reliance on standard FFT/IFFT operations make it well-suited for hardware implementation using existing digital signal processing (DSP) platforms. The improved BER performance at lower SNR values further highlights the robustness of the proposed scheme. Its ability to operate without prior channel knowledge or pilot signals reduces synchronization overhead and enhances spectral efficiency in 5G NR CP-OFDM frameworks. Future research could focus

on extending the proposed timing detection scheme to other MIMO configurations and exploring its performance in more complex channel conditions, such as those encountered in high-mobility scenarios. Additionally, integrating this method with other signal processing techniques, like machine learning algorithms, could further enhance its accuracy and efficiency. Investigating the applicability of the proposed scheme in different modulation schemes and error-correction codes could also provide valuable insights into its versatility across various communication standards. While the proposed method shows strong performance, it assumes ideal synchronization conditions aside from timing offset and uses a simplified doubly dispersive channel model. Limitations may arise under extreme operating scenarios. At very low SNR, although subcarrier averaging helps suppress noise, residual estimation variance may still cause occasional timing ambiguity. In the presence of large CFO values beyond half the subcarrier spacing, additional coarse acquisition may be required, as the estimator is designed for fine synchronization. Real-world deployment may also face additional challenges such as hardware impairments, rapidly time-varying Doppler shifts, and limited processing resources. Furthermore, the current implementation is offline and simulation-based; practical deployment would require efficient real-time realization. Future work could also explore hardware implementation and extend the algorithm to more complex channel scenarios, including higher mobility and carrier aggregation setups.

REFERENCES

Boodai, J., Alqahtani, A., & Frikha, M. (2023). Review of Physical Layer Security in 5G Wireless Networks. *Applied Sciences (Switzerland)*, ***13***(12). doi:10.3390/app13127277

Chen, W., Lin, X., Lee, J., Toskala, A., Sun, S., Chiasserini, C. F., & Liu, L. (2023). 5G-Advanced Toward 6G: Past, Present, and Future. *IEEE Journal on Selected Areas in Communications*, ***41***(6). doi:10.1109/JSAC.2023.3274037

Fazel, K., & Kaiser, S. (2008). Multi-Carrier and Spread Spectrum Systems. In *Multi-Carrier and Spread Spectrum Systems*. doi:10.1002/9780470714249

Ji, H., Park, S., Yeo, J., Kim, Y., Lee, J., & Shim, B. (2018). Ultra-Reliable and Low-Latency Communications in 5G Downlink: Physical Layer Aspects. *IEEE Wireless Communications*, ***25***(3). doi:10.1109/MWC.2018.1700294

Jin, H., Liu, K., Zhang, M., Zhang, L., Lee, G., Farag, E. N., Zhu, D., Onggosanusi, E., Shafi, M., & Tataria, H. (2023). Massive MIMO Evolution Toward 3GPP Release 18. *IEEE Journal on Selected Areas in Communications*, ***41***(6). doi:10.1109/JSAC.2023.3273768

Kalbat, F., Al-Dweik, A., & Ahmed, A. (2022). On the Performance of Precoded OFDM Systems in the Presence of Symbol Timing Offset. *IEEE Transactions on Vehicular Technology*, ***71***(9). doi:10.1109/TVT.2022.3176007

Kang, Y., Kim, S., Ahn, D., & Lee, H. (2008). Timing estimation for OFDM systems by using a correlation sequence of preamble. *IEEE Transactions on Consumer Electronics*, ***54***(4). doi:10.1109/TCE.2008.4711208

Kojima, S., Goto, Y., Maruta, K., Sugiura, S., & Ahn, C. J. (2023). Timing Synchronization Based on Supervised Learning of Spectrogram for OFDM Systems. *IEEE Transactions on Cognitive Communications and Networking*, ***9***(5). doi:10.1109/TCCN.2023.3280159

Lin, D. W. (2018). An Analysis of the Performance of ML Blind OFDM Symbol Timing Estimation. *IEEE Transactions on Signal Processing*, ***66***(20). doi:10.1109/TSP.2018.2868043

Ling, F., & Proakis, J. (2017). Synchronization in Digital Communication Systems. In *Synchronization in Digital Communication Systems*. doi:10.1017/9781316335444

Liu, D., Luo, Y., Li, Y., Wang, Z., Li, Z., Zhang, Q., Zhang, J., & Li, Y. (2022). An LDPC Encoder Architecture with Up to 47.5 Gbps Throughput for DVB-S2/S2X Standards. *IEEE Access*, ***10***.

doi:10.1109/ACCESS.2022.3151086

Liu, T., & Zhou, X. (2009). Joint blind estimation of symbol timing offset and carrier frequency offset for OFDM systems with I/Q imbalance. *IEICE Electronics Express*, ***6***(8). doi:10.1587/elex.6.443

Ma, S., Pan, X., Yang, G. H., & Ng, T. S. (2009). Blind symbol synchronization based on cyclic prefix for OFDM systems. *IEEE Transactions on Vehicular Technology*, ***58***(4). doi:10.1109/TVT.2008.2004031

Matin, S. A., & Milstein, L. B. (2021). OFDM System Performance, Variability and Optimality with Design Imperfections and Channel Impediments. *IEEE Transactions on Vehicular Technology*, ***70***(1). doi:10.1109/TVT.2020.3044665

Nasir, A. A., Durrani, S., & Kennedy, R. A. (2010). Performance of coarse and fine timing synchronization in OFDM receivers. *Proceedings of the 2010 2nd International Conference on Future Computer and Communication, ICFCC 2010*, *2*. doi:10.1109/ICFCC.2010.5497461

Peng, G., Li, R., He, Y., & Han, Z. (2023). Timing and Frequency Synchronization Using CAZAC Sequences for OFDM Systems. *Sensors*, ***23***(6). doi:10.3390/s23063168

Sarwar, M. S., Ahmad, M., & Shin, S. Y. (2023). Subcarrier Index Modulation for Spectral Efficient Frequency Division Multiplexing in Multi-Input Multi-Output Channels. *IEEE Transactions on Vehicular Technology*, ***72***(2). doi:10.1109/TVT.2022.3213011

Shammaa, M., Mashaly, M., & El-Mahdy, A. (2024). The Use of Deep Learning Techniques in OFDM Receivers for 5G NR: A Survey. *Procedia Computer Science*, ***231***. doi:10.1016/j.procs.2023.12.154

Suyoto, Subekti, A., Satyawan, A. S., Mardiana, V. A., Armi, N., & Kurniawan, D. (2021). Performance analysis of OFDM-IM scheme under STO and CFO. *International Journal of Electrical and Computer Engineering*, ***11***(4). doi:10.11591/ijece.v11i4.pp3293-3299

Tang, Z. (2023). OFDM communication system based on FPGA. *Proceedings - 2023 3rd Asia-Pacific Conference on Communications Technology and Computer Science, ACCTCS 2023*. doi:10.1109/ACCTCS58815.2023.00126

Van De Beek, J. J., Sandell, M., & Börjesson, P. O. (1997). ML estimation of time and frequency offset in OFDM systems. *IEEE Transactions on Signal Processing*, ***45***(7). doi:10.1109/78.599949

Wang, M. M., Xiao, L., Brown, T., & Dong, M. (2009). Optimal symbol timing for OFDM wireless communications. *IEEE Transactions on Wireless Communications*, ***8***(10). doi:10.1109/TWC.2009.090263

Wang, Y. C., & Phoong, S. M. (2017). Blind estimation of symbol timing offset in OFDM systems. *IEEE Workshop on Signal Processing Advances in Wireless Communications, SPAWC, 2017-July*. doi:10.1109/SPAWC.2017.8227808

Yağlı, K., & Aldırmaz Çolak, S. (2022). Preamble-Based Symbol Timing Algorithms in OFDM Systems. *The European Journal of Research and Development*, ***2***(2). doi:10.56038/ejrnd.v2i2.91

Yang, C., Wang, L., Peng, C., Zhang, S., Cui, Y., & Ma, C. (2024). A Robust Time-Frequency Synchronization Method for Underwater Acoustic OFDM Communication Systems. *IEEE Access*, *12*. doi:10.1109/ACCESS.2024.3361845

Yang, F., & Zhang, X. (2024). An Efficient Symbol Timing Scheme for OFDM Systems Using Optimal Correlation-Based Circular-Shifted Preamble. *IEEE Wireless Communications Letters*. doi:10.1109/LWC.2019.2944154

Yang, J., Jiang, Y., Zhu, X., Sun, D., Wang, T., & Zheng, F. (2020). Blind Timing Synchronization for DCO-OFDM VLC Systems. *Proceedings - IEEE Global Communications Conference, GLOBECOM*. doi:10.1109/GLOBECOM42002.2020.9322214

Yli-Kaakinen, J., Loulou, A., Levanen, T., Pajukoski, K., Palin, A., Renfors, M., & Valkama, M. (2021). Frequency-Domain Signal Processing for Spectrally-Enhanced CP-OFDM Waveforms in 5G New Radio. *IEEE Transactions on Wireless Communications*, ***20***(10). doi:10.1109/TWC.2021.3077762

Yusof, A., Idris, A., & Abdullah, E. (2023).

Papr Reduction in CP-OFDM (5g) Using Hybrid Technique. *Acta Polytechnica*, ***63***(5). doi:10.14311/AP.2023.63.0364

Zhang, J., & Liu, Y. (2023). Research of Time-Frequency Synchronization Technology Based on OFDM System. *2023 4th International Symposium on Computer Engineering and Intelligent Communications, ISCEIC 2023*. doi:10.1109/ISCEIC59030.2023.10271100